IIETA International Information and Engineering Technology Association
Advancing the World of Information and Engineering

Journal Européen des Systèmes Automatisés
Vol. 57, No. 5, October, 2024, pp. 1321-1328
Journal homepage: http://iieta.org/journals/jesa

Identification and Classification of Power Quality Disturbances via Synchro-Reassigning Transform

Roshan Kumar[1], Vikash Singh[2*], Anuj Baral[2], Swati Varun Yadav[2]

[1] Department of Electronic and Information Technology, Miami College of Henan University, Kaifeng 475004, China
[2] Department of Instrumentation and Control Engineering, Manipal Institute of Technology, Manipal Academy of Higher Education, Manipal 576104, India

Corresponding Author Email: vikash.nepal@manipal.edu

https://doi.org/10.18280/jesa.570507

Received: 14 March 2024
Revised: 15 August 2024
Accepted: 29 August 2024
Available online: 28 October 2024

Keywords:
STFT, WT, SST, SRT, PQ

ABSTRACT

This study introduces the Synchro-Reassigning Transform (SRT), a cutting-edge method developed for high-resolution time-frequency analysis of power quality (PQ) disturbances. The research assesses the performance of SRT in comparison to other established techniques such as Short-Time Fourier Transform (STFT), Wavelet Transform (WT), Synchro-Squeezing Transform (SST), and Synchro-Extracting Transform (SET). Specifically, the study focuses on the identification and categorization of various PQ issues, including voltage sags, swells, interruptions, harmonics, and inter-harmonics. The analysis reveals that SRT excels in detecting harmonics and inter-harmonics, providing much clearer and more detailed time-frequency representations by minimizing cross-term interference, which is a limitation often observed in other methods. The results highlight SRT's ability to offer more accurate and reliable signal interpretations, leading to enhanced precision in PQ analysis. Overall, this technique represents a significant advancement in power quality monitoring, delivering greater reliability and improving the accuracy of PQ disturbance detection.

1. INTRODUCTION

The world has rapidly industrialized during the last two decades. The use of sensitive equipment with non-linear loads is on the rise in industries as well as commercial sectors [1]. The increasing use of such equipment as well as the integration of renewable energy sources into the power system are some of the primary reasons for PQ disturbances [2]. The presence of harmonics, inter-harmonics, voltage sag, swell, flickers, and distortion in power signals is known as PQ disturbance. It may damage equipment, reduce process and product quality, interrupt production, and cause safety issues [1, 3]. As per the PQ survey of industrial customers conducted in the US in 2000. It was reported that the most adversely impacted equipment are computers and microprocessor-based equipment (43%), variable speed drives (13%), lighting equipment (8%), motors (5%), relays (1%), and other equipment (30%) [4]. PQ disturbance should be mitigated to avoid financial and physical losses. With the help of modern signal processing tools identification and localization of PQ disturbances can be easily done [5]. In this regard, much research has been done, and a brief history and review of those methods are presented here.

The problem of identifying power quality disruptions has been extensively studied using various signal processing techniques, including STFT, WT, S-transform (ST), Wigner-Ville distribution (WVD), Gabor-Wigner transform (GWT), Hilbert-Huang transform (HHT), and Synchro-squeezing transform (SST) [5-12]. The traditional STFT method converts a one-dimensional time-domain signal into a two-dimensional time-frequency (TF) plane. This is done by segmenting a non-stationary signal into smaller, quasi-stationary segments using a window function. The frequency spectrum for each segment is then determined through the Fourier transform. However, a significant limitation of this method is that the TF resolution is dependent on the window size. A smaller window provides better time resolution, while a larger window offers better frequency resolution. Thus, achieving an optimal balance between temporal and frequency resolution necessitates the careful selection of the appropriate window size, a process that can be particularly challenging and laborious.

The WT uses the adjustable window size to circumvent this shortcoming of STFT [13-15]. The TF plane produced by this method is blurry due to the Heisenberg uncertainty principle. Apart from this, the TF resolution depends on the selection of the mother wavelet [16, 17]. The lower orders of Daubechies's wavelets are good at detecting fast transients, while the higher orders are good at detecting slow changes [8].

In PQ analysis, fast and slow changes were identified; this method may not be suitable for this purpose. Further, lifting-based wavelet filters (LBWT) were proposed for the analysis of PQ events in reference [17], where it was demonstrated that LBWT is more suitable for hardware implementation than traditional WT [18]. A teager energy operator (TEO) based algorithm for PQ event detection has been introduced in reference [19]. The TEO-based method is shown to be quick

and reliable in detecting voltage disturbances.

The WVD is one of the widely used methods in digital signal processing applications. It offers good TF resolution for mono-frequency signals, but its application is constrained by the presence of cross-terms in the TF plane, which hinders the detection of harmonics and inter-harmonics components present in the PQ signal. Pei and Ding [8] proposed GWT to investigate PQ disturbance events and through numerical analysis proved that it has better TF resolution than that of GT and WVD [20]. To improve TF resolution, S-transform is introduced in reference [4], which is formed by combining STFT and WT. Although ST improves TF resolution; however, its resolution is limited when the Gaussian window is used [7]. In reference [21], PQ disturbance analysis was carried out using STFT, SST, and SET methods and reported that SET has the least Renyi entropy and the sharpest TF resolution among all. Motivation and organization of the paper.

Accurate detection and classification of PQ disturbances are vital for maintaining the reliability of electrical grids. TF analysis methods like Short-Time Fourier STFT, GT, and WT are limited by their reliance on precise window size selection and the Heisenberg uncertainty principle, which restricts resolution [22]. While the SET improves TF resolution, it still struggles with nonlinear signals and cross-term interference, resulting in unclear representations.

This study introduces the SRT as an innovative solution for detecting and classifying PQ disturbances, especially in environments with nonlinear signals and noise. SRT excels by reducing cross-term interference and delivering precise TF representations, surpassing traditional methods like STFT, WT, and SET in various PQ scenarios and across different signal-to-noise ratios (SNRs). The lower Renyi entropy of SRT underscores its superior TF resolution, establishing it as a robust tool for PQ disturbance analysis [23].

The structure of this paper is as follows: Section 2 reviews the TF methods utilized in this research. Section 3 explores the mathematical foundation of Renyi entropy and its importance in evaluating TF techniques. Section 4 presents the results of our analysis, and Section 5 concludes the study with key findings and implications.

2. TIME-FREQUENCY APPROACH

This section offers a thorough overview of various TF techniques. Furthermore, it delves into the underlying principles, algorithms, and essential components of each method, providing a comprehensive understanding of their functioning.

2.1 STFT

STFT, which is also known as a windowed FT, was first introduced by Dennis Gabor in 1946 to overcome the constraints of FT. In this technique, the signal is converted from a one-dimensional space into a two-dimensional time-frequency plane, where each box is referred to as a Heisenberg box. Changing the window functions can change the time-frequency resolution. Various kinds of window functions evolved to divide the signal into smaller portions. Each window function has pros and cons of its own. The resolution is significantly influenced by the window width, FFT size, and time shift (also known as the hope number) [13].

The mathematical representation of STFT is expressed as:

$$STFT_x(\omega,t)=\int_{-\infty}^{\infty} f(u)w(u-t)e^{-j\omega(u-t)}du \tag{1}$$

where $f(u)$ is a time-domain signal, $w(u)$ is a window function and t indicate the position of the window. Eq. (1) provides a time-frequency representation of the windowed signal.

2.2 SET

SET, introduced by Yu et al. [24], offers a more energy-concentrated time-frequency representation compared to other techniques. This method operates on the assumption that multicomponent signals are composed of a sum of several non-stationary modes.

$$f(t)=\sum_{k=1}^{n} a_k(t)e^{im_k(t)} \tag{2}$$

where the instantaneous amplitude and instantaneous phase are denoted by $a(t)$ and $m(t)$, respectively. These modes are distinct and separated by a certain distance.

$$m'_{k+1}(t)-m'_k(t)>2\Delta \tag{3}$$

STFT is further expressed in the discrete domain,

$$STFT(t,\omega)=\sum_{k=1}^{n} a_k(t)g\big(\omega-m'_k(t)\big)e^{jm_k(t)} \tag{4}$$

Furthermore, the instantaneous frequency can be represented as follows:

$$m'(t,\omega)=-i\frac{\partial_t STFT(t,\omega)}{STFT(t,\omega)} \tag{5}$$

Most of the smeared signals on the time-frequency plane are effectively eliminated by SET, allowing the expression to be defined as follows:

$$SET(t,\omega)=STFT(t,\omega).\partial\big(\omega-m'(t,\omega)\big) \tag{6}$$

Further, the above equation can be expressed.

$$SET(t,\omega)=\begin{cases}STFT(t,\omega) & \omega=\omega_0\\ 0, & \omega\neq\omega_0\end{cases} \tag{7}$$

Finally, the mathematical expression for SET can be represented as follows:

$$\begin{aligned}&SET(t,\omega)|_{\omega-\sum_{k=1}^{n} m_k(t)=0}\\ &=STFT(t,\omega)|_{\omega-\sum_{k=1}^{n} m_k(t)=0}\end{aligned} \tag{8}$$

2.3 WT and its variant SST

The term wave denotes that the function is oscillatory, while the word wavelet refers to a small wave. By keeping the window width constant, Morlet observed that the STFT approach did not perform well. In the studies [22, 25], to address the limitations of STFT, the wavelet transform concept was developed, incorporating methods of scaling and shifting window functions. The mathematical expression for the

wavelet transform is as follows:

$$WT_s(s,b) = \frac{1}{\sqrt{s}} \int f(u) \emptyset^* \left(\frac{u-b}{s}\right) du \tag{9}$$

The wavelet response of the signal often results in blurred information across the time-frequency plane, potentially leading to misleading results. To mitigate this blurring effect, Daubechies et al. [26] proposed a synchro-squeezing algorithm. This algorithm reduces the blurring and determines the instantaneous frequency (s, b) by computing the derivative of the wavelet transform $WT_s(s,b)$ with respect to b.

$$\omega_s(s,b) = \frac{-i}{2\pi WT_s(s,b)} \frac{\partial WT_s(s,b)}{\partial b} \tag{10}$$

The operation of every point (s, b) reassigning to $(b, Ws\ (s, b))$ is known as synchro squeezing. Define frequency divisions $\omega_l \in [0, \infty)$, where $\omega_0 > 0$ and $\omega_{l+1} > \omega_l$.

$$T_s(w_l, b) = \int\limits_{\{s:w_s(s,b)\in F_l\}} WT_s(s,b) s^{\frac{-3}{2}} ds \tag{11}$$

The response computed from SST is highly concentrated on the time-frequency plane, but cross-terms can still be observed in the results.

2.4 SRT

The STFT is the first fundamental TF method in which the signal is decomposed into different segments and the fast FT of each chunk is computed at each time interval. It can be expressed as

$$STFT_x(\omega,t) = \int_{-\infty}^{\infty} f(u) w(u-t) e^{-j\omega(u-t)} du \tag{12}$$

where, $f(u)$ is a time-domain signal, $w(u)$ is a window function and t indicate the position of the window. Fourier transform is computed for a certain part of the window with a time centre.

$$STFT_x(\omega,t) = \int_{t-\Delta u}^{t+\Delta u} f(u) w(u-t) e^{-j\omega(u-t)} du \tag{13}$$

where, Δu is half of the window length.

$$STFT_x(\omega,t) = Re(STFT_x) + Im(STFT_x) \tag{14}$$

Eq. (14) is further simplified and obtains the magnitude of

$$P = |STFT_x(\omega,t)| = \sqrt{Re(STFT_x)^2 + Im(STFT_x)^2} \tag{15}$$

The first order derivative of Eq. (15) with respect to ω.

$$\frac{\partial P}{\partial \omega} = \frac{Re(STFT_x)\frac{\partial Re(STFT_x)}{\partial \omega} + Im(STFT_x)\frac{\partial Im(STFT_x)}{\partial \omega}}{|STFT_x(\omega,t)|} \tag{16}$$

Now, compute the first derivative of Eq. (13) with respect to ω.

$$STFT'_{x,\omega}(\omega,t) = \frac{\partial STFT_x(\omega,t)}{\partial \omega} \tag{17}$$

$$STFT'_{x,\omega}(\omega,t) = Re\{(STFT\}'_{x,\omega}) + Im j\{(STFT\}'_{x,\omega}) \tag{18}$$

By implementing a similar operation on Eq. (18), we obtain

$$STFT'_{x,\omega}(\omega,t) = \frac{\partial Re(STFT_x)}{\partial \omega} + j\frac{\partial Im(STFT_x)}{\partial \omega} \tag{19}$$

Comparing Eq. (18) and Eq. (19):

$$\frac{\partial Re(STFT_x)}{\partial \omega} = Re\{(STFT\}'_{x,\omega}) \tag{20}$$

$$\frac{\partial \{Im(STFT\}_x)}{\partial \omega} = Im\{(STFT\}'_{x,\omega}) \tag{21}$$

From Eq. (20) and Eq. (21), Eq. (16) is modified.

$$\frac{\partial P}{\partial \omega} = \frac{Re(STFT_x)Re(STFT'_{x,\omega}) + Im(STFT_x)Im\,(STFT'_{x,\omega})}{|STFT_x(\omega,t)|} \tag{22}$$

$$P'(a,b) = \frac{\partial P}{\partial \omega} = \frac{Re\big(STFT_x(a,b)\big)Re(STFT'_{x,\omega}(a,b)) + Im(STFT_x(a,b))Im\,(STFT'_{x,\omega}(a,b))}{|STFT_x(a,b)|} \tag{23}$$

where, a is the discrete frequency center, $a=0,1,2,\ldots,L$, L is the length of the window function, b is the discrete-time center, STFx (a, b) is a discrete form of Eq. (12), and $STFTx$, $\omega'(a, b)$ is a partial derivative of STFx (a, b).

To compute the Synchro-Reassigning Transform, the following conditions must be satisfied.

$$\begin{Bmatrix} |STFT_x(a-1,b)| \le |STFT_x(a,b)| \\ |STFT_x(a+1,b)| \le |STFT_x(a,b)| \end{Bmatrix} \tag{24}$$

$$\begin{Bmatrix} |P'(a,b)| < e_{cal} \\ |P'(a,b)| \le |P'(a-1,b)| \\ |P'(a,b)| \le |P'(a+1,b)| \end{Bmatrix} \tag{25}$$

$$\begin{Bmatrix} P'(a,b) < P'(a-1,b) \\ P'(a,b) > P'(a-1,b) \end{Bmatrix} \tag{26}$$

The Eqs. (24)-(26) are utilized to calculate local maxima that re-assign the new coefficients and evolved a new time-frequency transform called SRT [23].

$$SRT(a,b) = \begin{cases} STFT_x(a,b); \\ If\ Eqs.(24)-(26)\ satisfied \\ 0; \qquad otherwise \end{cases} \tag{27}$$

The effectiveness of SRT in PQ analysis stems from its unique properties. It enhances time-frequency resolution by redistributing energy to its correct time-frequency coordinates, which leads to a more accurate and concentrated representation. This capability is crucial for analyzing disturbances that exhibit rapid changes or non-stationary

behavior. Additionally, SRT's reduction of cross-term interference ensures that the time-frequency representations remain sharp and clear, particularly when dealing with signals that have closely spaced frequencies. These characteristics make SRT particularly well-suited for PQ analysis, where precision is essential.

3. STATISTICAL ANALYSIS OF TIME-FREQUENCY METHOD: RENYI ENTROPY

In many cases, visual inspection may not provide consistent results, prompting the need for an objective evaluation method to determine the best time-frequency approach. This research work employs Renyi entropy for identifying the appropriate time-frequency method. Renyi entropy was introduced by Rényi [27], it provides insights about how information is distributed inside a system. In the field of signal processing, it is the most employed measure to quantify the TF resolution of the TF analysis schemes [14, 24, 28]. The Reyni entropy can be written as

$$R_\alpha = \frac{1}{1-\alpha} log \int_{-\infty}^{+\infty} \int_{-\infty}^{+\infty} \rho^\alpha{}_{norm}(t,f) dtdf \qquad (28)$$

Here $\alpha = 3$ is selected for analysis, ρ^α is normalized time-frequency distribution can be expressed as:

$$\rho_{norm}(t,f) = \frac{\rho(t,f)}{\int_{-\infty}^{+\infty} \int_{-\infty}^{+\infty} \rho(t,f) dtdf} \qquad (29)$$

Renyi entropy is used in this study to objectively compare different TF analysis methods. Subtle variations in TF representations can be challenging to assess visually, making it difficult to determine which method is most effective. Renyi entropy provides a numerical measure of how concentrated the energy is in the time-frequency plane, with a lower value indicating a clearer and more focused representation. In this research, Renyi entropy serves as a critical metric for evaluating and distinguishing between TF methods, with the approach yielding the lowest entropy identified as offering the most accurate time-frequency analysis.

4. RESULT AND ANALYSIS

This section compares the effectiveness of several TF analysis techniques using a variety of well-documented PQ disturbance events, such as voltage sag, swell, interruption, harmonics, and inter-harmonics simulated in MATLAB. In subsections 4.1 to 4.4, mathematical equations for each PQ disruption event are mentioned. For simplicity of analysis, generated input signals are normalized at the input stage.

For the sake of simulation, we have considered a window size of 64 samples, a sinusoidal voltage of 50 Hz, and a sampling frequency of 103 Hz. Unless otherwise stated, these parameters are used for numerical analysis throughout the study.

4.1 Voltage sag

The equation for instantaneous voltage sag is described in Eq. (30) and shown in Figure 1(a), where the voltage magnitude temporarily decreases by a factor of β resulting in an amplitude reduction to $(1-\beta) = 0.5$, indicating 50% voltage drop. The voltage sag is sustained for 0.1 seconds.

$$(f_s(t) = [1 - \beta u(t-t_1) - u(t-t_2)] \sin(\omega t)) \qquad (30)$$

where, $0.1 \leq \beta \leq 0.9$ and $T \leq t_2 - t_1 \leq 9T$.

In this equation, t_1 represents the moment when the voltage begins to decline from its normal level, initiating the voltage sag. Conversely, t_2 marks the point when the voltage recovers back to its original level. The time interval between t_1 and t_2 specifies the duration of the sag, which, for this case, is set at 0.1 seconds. The normalized waveform and the corresponding TF analysis results are depicted in Figures 1 and 2. In these figures, the voltage sag is observable as a lighter segment between 0.4 seconds and 0.5 seconds, where the voltage is lower than the normal level. This event is classified as a voltage sag. The TF resolution, shown in ascending order of clarity in Figure 1(b)-Figure 2(c), illustrates how different TF methods capture this disturbance, with the SRT method providing the most precise representation.

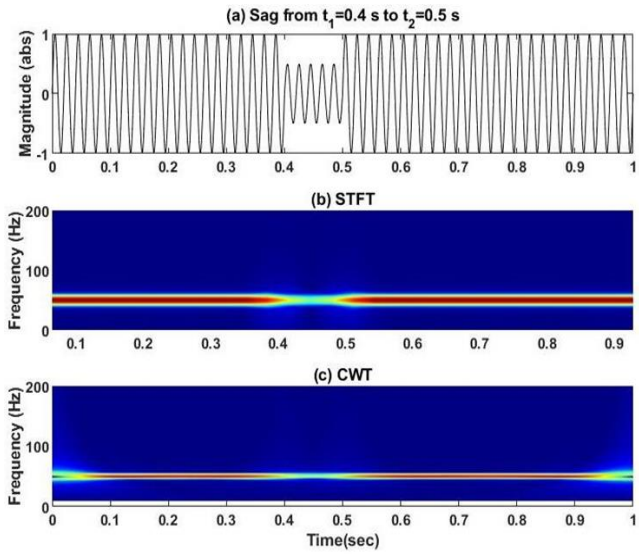

Figure 1. (a) For voltage sag (b) STFT (c) WT

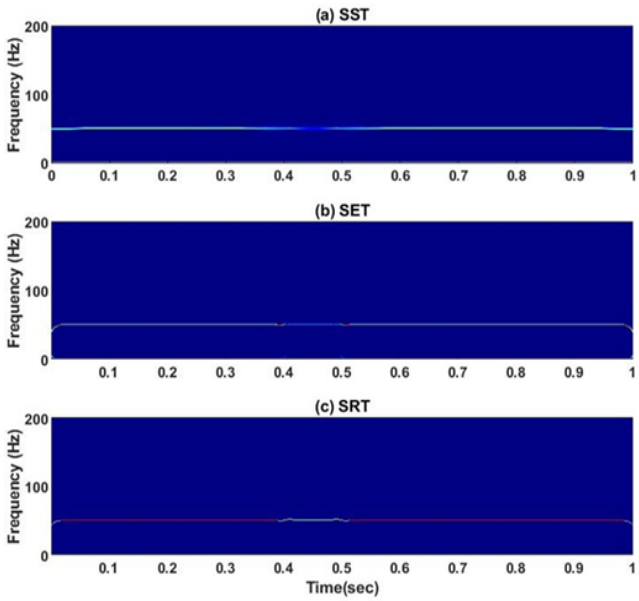

Figure 2. For voltage sag (a) SST (b) SET (c) SRT

Among all the TF techniques, STFT and WT exhibit lower TF resolution due to their susceptibility to the Heisenberg uncertainty principle. Consequently, they experience a "blurring" or 'smearing out' effect in their TF representation [24, 29]. In contrast to STFT and WT, SST offers improved TF resolution. It is categorized as a special reassignment method that compresses WT coefficients along the IF trajectory in the frequency direction exclusively. Additionally, the TF resolution can be further enhanced by utilizing SET. The improved energy concentration of the TF representation in SET results from retaining the maximum value of STFT's TF coefficient to generate a new TF representation. Unlike SST, which compresses the TF coefficients, SET extracts the maximum TF coefficients, leading to its distinct advantage.

In this study, SRT is employed to improve the TF resolution of PQ disturbance events. SRT utilizes derivatives of the constructed amplitude function and a three-step selection rule to dynamically identify TF coefficients along the IF trajectories in the time-frequency plane. These coefficients are then reassigned to a new TF plane. Consequently, SRT allows for more accurate IF estimation, leading to enhanced time-frequency resolution.

4.2 Voltage swell

The mathematical expression for instantaneous voltage swell is given in Eq. (31). The instantaneous voltage swells with magnitudes $(1+\beta)$=1.8 (i.e., the magnitude of 80%) and time duration of 0.15 seconds is analysed using various TF approaches, like, STFT, WT, SST, SET, and SRT.

$$f_{w(t)} = [1 + \beta\, u(t - t_1) - u(t - t_2)]sin(\omega t) \qquad (31)$$

where, $0.1 \leq \beta \leq 0.8$ and $T \leq t_2 - t_1 \leq 9T$.

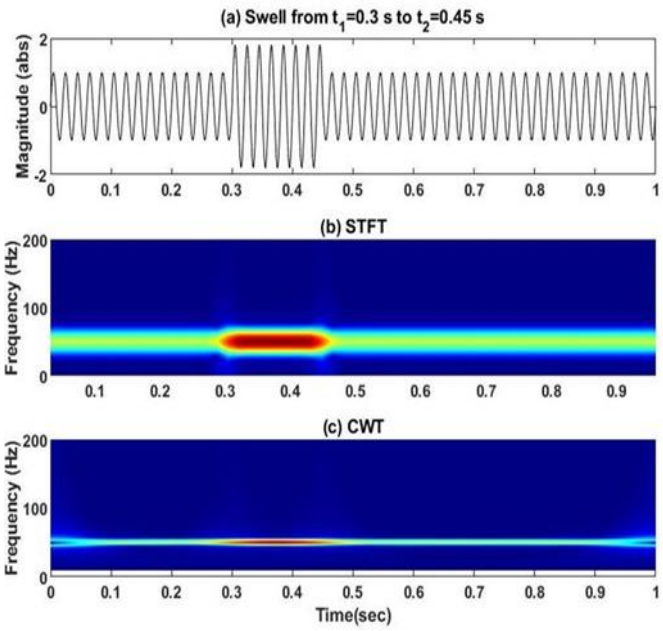

Figure 3. (a) Voltage swell (b) STFT (c) WT

The time domain of the normalized waveform and the figure for TF results are shown in Figure 3, and Figure 4, respectively, where the darker part starts at 0.3 second and end at 0.45 second, which indicates that the instantaneous voltage level is higher than the normal voltage level during the mentioned period (from 0.3 to 0.45sec), identifying this PQ event as voltage swells. The Renyi entropy plot and the TF graphs in Figures 3 and 4 show that SRT has the best TF resolution, making it the best tool for locating voltage sag occurrences.

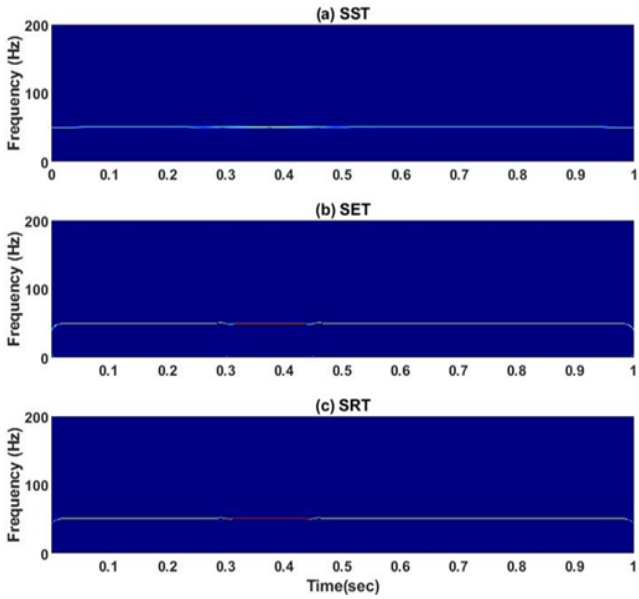

Figure 4. For voltage swell (a) SST (b) SET (c) SRT

4.3 Voltage interruption

The expression for instantaneous voltage interruption is mentioned in Eq. (32). In this subsection, the TF analysis of the instantaneous voltage interruption with zero magnitudes and a time duration of 0.2 seconds is carried out with STFT, WT, SST, SET, and SRT.

$$f_{t(t)} = [1 - \beta u(t - t_1) - u(t - t_2)]sin(\omega t) \qquad (32)$$

where, $0.9 \leq \beta \leq 0.1$ and $T \leq t_2 - t_1 \leq 9T$.

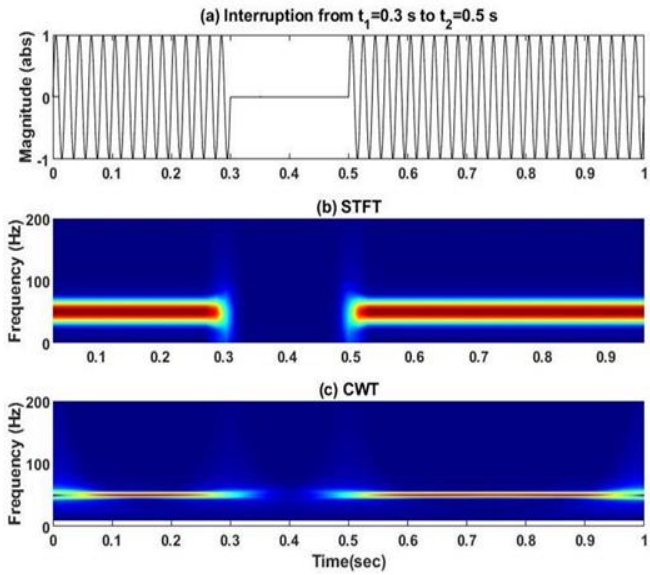

Figure 5. (a) Voltage interruption (b) STFT (c) WT

The figures for voltage interruption and the TF analysis results are shown in Figure 5 and Figure 6, respectively. In the TF figure, the blank part starts at 0.3 second and ends at 0.5

second, which shows the voltage interruption, classifying this PQ disturbance event as voltage interruption. By carefully examining the Renyi entropy shown in Figure 7 and the figures for various TF analyses displayed in Figures 5 and 6, it is observed that all the observations mentioned in the preceding subsection for SRT also hold for this case. As a result, we can say that it is the best TF approach for classifying voltage interruption events.

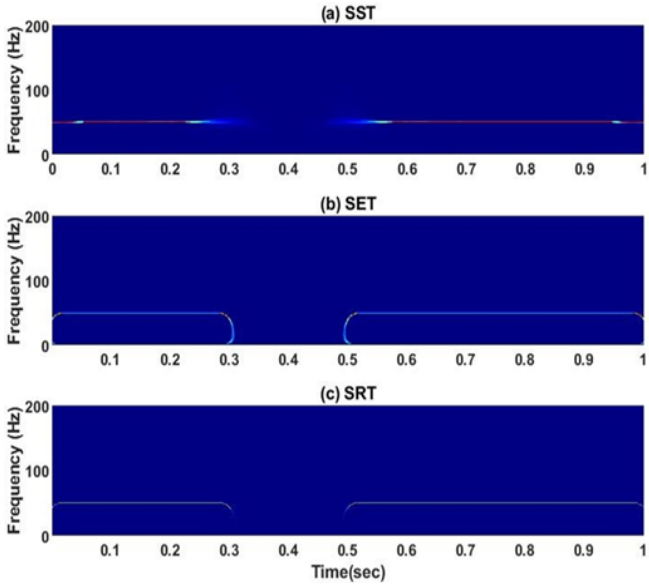

Figure 6. For voltage interruption (a) SST (b) SET (c) SRT

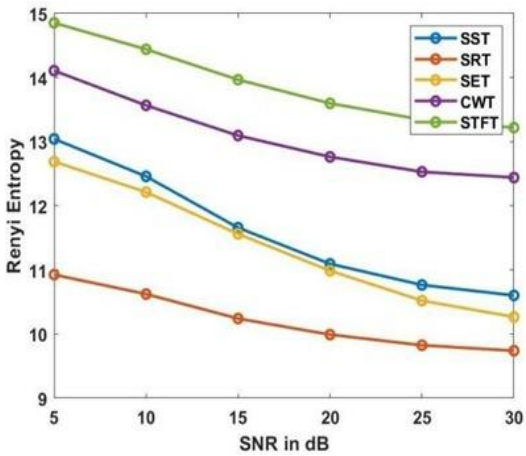

Figure 7. The Renyi entropy values of the TFR generated by STFT, WT, SET, SRT, and SST under different noise levels of the voltage interruption

4.4 Harmonics and inter-harmonics

In Eq. (33), a voltage waveform with a third harmonic of 150 Hz and an inter-harmonic of 100 Hz is mentioned. The signal in Eq. (33) is analysed with STFT, WT, SST, SET, and SRT, respectively for a window length of 128 samples. Here, the window length is increased to account for harmonics and inter-harmonic components.

$$f_h(t) = sin(2\pi ft) + u(t - t_1)[\beta_1 sin(2\pi 3f) + \beta_2 sin(2\pi 2f)] \quad (33)$$

where, $\beta_1 = 0.3$, $\beta_2 = 0.1$, and $t_1 = 0.5$.

The time domain and TF plot of Eq. (33) are shown in Figures 8 and 9.

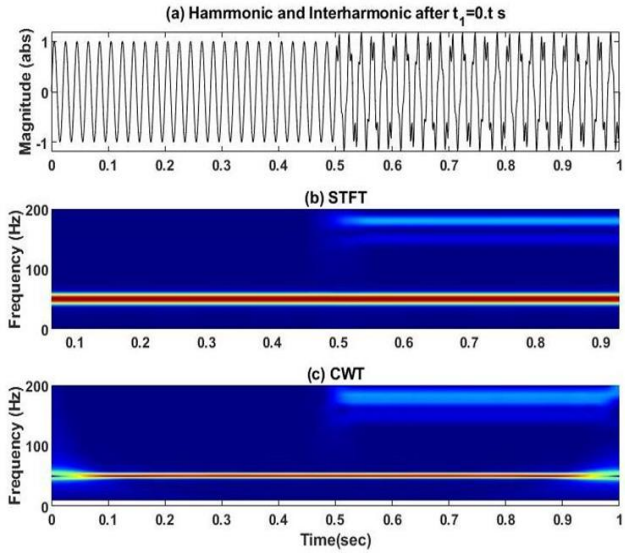

Figure 8. (a) Harmonics and Inter-harmonics (b) STFT (c) WT

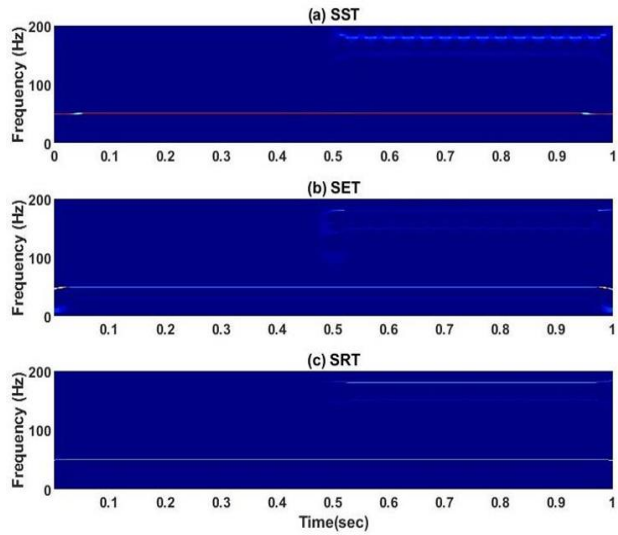

Figure 9. For Harmonics and Inter-harmonics (a) SST (b) SET (c) SRT

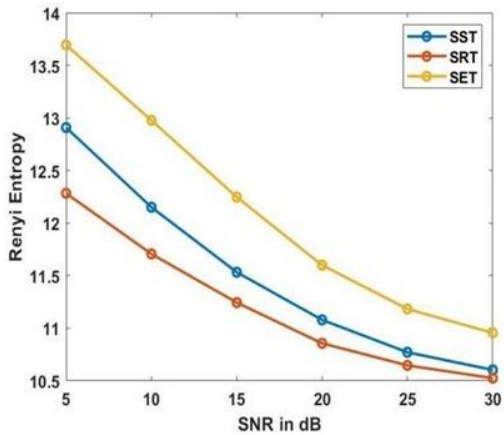

Figure 10. The Renyi entropy values of the TFR generated by SET, SRT, and SST under different noise levels of the voltage harmonics and inter-harmonics

From the figures, it can be observed that the TF resolution of SRT is better than the rest. The Renay entropy shown in Figure 10 also substantiates the claim. From Figure 9 we can observe that in the case of SET Figure 8(b), TF resolution of harmonic and inter-harmonic is not as sharp as compared to SRT (i.e., Figure 9(c)). Thus, we can claim that SRT is the best TF approach to identify harmonics and inter-harmonics in PQ disturbance analysis.

4.5 Performance analysis of TF methods under disturbances

To test the performance of various time-frequency methods, additive white Gaussian noise with different SNR values is also added to the test signal to consider the effect of the field environment, and the Renyi entropy was calculated for each SNR value. The Renyi entropy is used as a performance indicator in this paper to assess the energy concentration of TF results. The higher the Renyi entropy value, the less energy is concentrated in the TF plane. The Renyi entropy for PQ disturbance signals with varying SNRs is calculated and plotted in Figure 9-12.

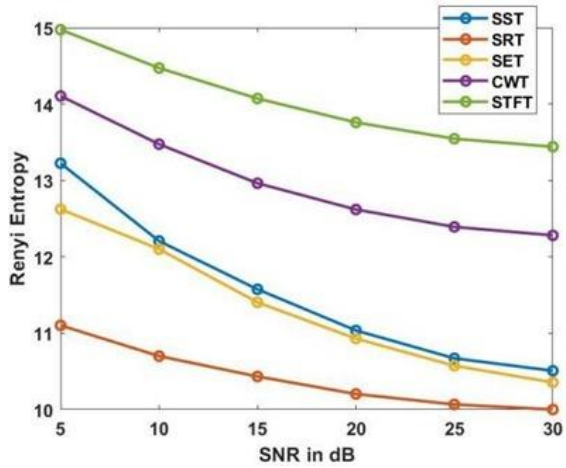

Figure 11. The Renyi entropy values of the TFR generated by STFT, WT, SET, SRT, and SST under different noise levels of the voltage sag

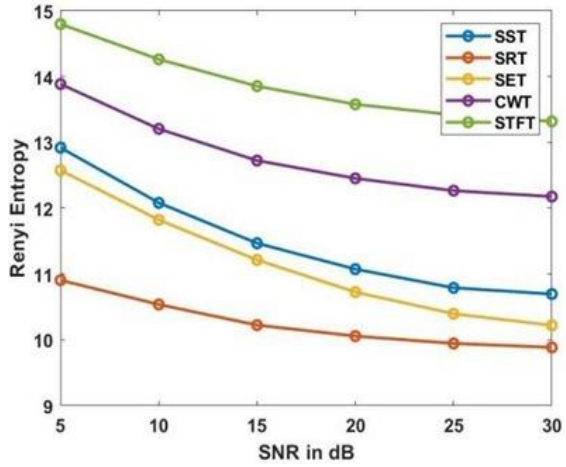

Figure 12. The Renyi entropy values of the TFR generated by STFT, WT, SET, SRT, and SST under different noise levels of the voltage swell

According to the figures, a lower value indicates a more energy-concentrated time-frequency representation. The Renyi entropy values increases as the noise strength increases. Irrespective of the SNR value and PQ disturbance signal, the SRT has minimum Renyi entropy, indicating that the SRT has higher energy concentration characteristics among all TF methods.

5. LIMITATIONS AND FUTURE RESEARCH DIRECTIONS

One limitation of SRT is its relatively high computational complexity, which can be a hindrance in real-time applications, especially within large-scale power systems where quick analysis is crucial. The processing demands of SRT may restrict its use in situations requiring immediate or near-instantaneous results.

Future research should explore ways to streamline the computational process of SRT. This could involve developing more efficient algorithms or leveraging parallel computing to speed up the time-frequency analysis. By addressing these computational challenges, SRT could be more effectively utilized in real-time power quality monitoring and management, broadening its practical applications.

6. CONCLUSIONS

This study establishes SRT as a highly effective tool for the detection and classification of PQ disturbances. Through a comparative analysis with methods such as STFT, WT, SST, and SET, SRT has proven to be particularly adept at identifying issues like voltage sags, swells, interruptions, harmonics, and inter-harmonics. Its ability to minimize cross-term interference leads to clearer and more accurate time-frequency representations. These outcomes suggest that SRT can play a crucial role in enhancing the precision and reliability of PQ analysis, which is essential for improving power quality monitoring and the overall management of power systems.

REFERENCES

[1] Stones, J., Collinson, A. (2001). Power quality. Power Engineering Journal, 15(2): 58-64. https://doi.org/10.1049/pe:20010201

[2] Bashawyah, D.A., Subasi, A. (2019). Power quality event detection using FAWT and bagging ensemble classifier. In 2019 IEEE International Conference on Environment and Electrical Engineering and 2019 IEEE Industrial and Commercial Power Systems Europe (EEEIC / I&CPS Europe), Genova, Italy, pp. 1-5. https://doi.org/10.1109/EEEIC.2019.8783281

[3] Santoso, S., Powers, E.J., Grady, W.M., Hofmann, P. (1996). Power quality assessment via wavelet transform analysis. IEEE Transactions on Power Delivery, 11(2): 924-930. https://doi.org/10.1109/61.489353

[4] Bhattacharyya, S., Cobben, S. (2011). Consequences of poor power quality–An overview. Power Quality. IntechOpen. https://doi.org/10.5772/13787

[5] Goswami, J.C., Chan, A.K. (2011). Fundamentals of Wavelets: Theory, Algorithms, and Applications. John Wiley & Sons.

[6] Mishra, S., Bhende, C.N., Panigrahi, B.K. (2007). Detection and classification of power quality disturbances using S-transform and probabilistic neural network. IEEE Transactions on Power Delivery, 23(1): 280-287. https://doi.org/10.1109/TPWRD.2007.911125

[7] Poisson, O., Rioual, P., Meunier, M. (2000). Detection and measurement of power quality disturbances using wavelet transform. IEEE transactions on Power Delivery, 15(3): 1039-1044. https://doi.org/10.1109/61.871372

[8] Pei, S.C., Ding, J.J. (2007). Relations between Gabor transforms and fractional Fourier transforms and their applications for signal processing. IEEE Transactions on Signal Processing, 55(10): 4839-4850. https://doi.org/10.1109/TSP.2007.896271

[9] Stockwell, R.G., Mansinha, L., Lowe, R.P. (1996). Localization of the complex spectrum: The S transform. IEEE Transactions on Signal Processing, 44(4): 998-1001. https://doi.org/10.1109/78.492555

[10] Afroni, M. J., Sutanto, D., Stirling, D. (2013). Analysis of nonstationary power-quality waveforms using iterative Hilbert Huang transform and SAX algorithm. IEEE Transactions on Power Delivery, 28(4), 2134-2144. https://doi.org/10.1109/TPWRD.2013.2264948

[11] Chen, S., Li, Z., Pan, G., Xu, F. (2022). Power quality disturbance recognition using empirical wavelet transform and feature selection. Electronics, 11(2): 174. https://doi.org/10.3390/electronics11020174

[12] Zhao, W., Shang, L., Sun, J. (2019). Power quality disturbance classification based on time-frequency domain multi-feature and decision tree. Protection and Control of Modern Power Systems, 4(1): 27. https://doi.org/10.1186/s41601-019-0139-z

[13] Kumar, R., Ismail, M., Zhao, W., et al. (2021). Damage detection of wind turbine system based on signal processing approach: A critical review. Clean Technologies and Environmental Policy, 23: 561-580. https://doi.org/10.1007/s10098-020-02003-w

[14] Kumar, R., Sumathi, P., Kumar, A. (2015). Analysis of frequency shifting in seismic signals using Gabor-Wigner transform. Earthquake Engineering and Engineering Vibration, 14: 715-724. https://doi.org/10.1007/s11803-015-0056-8

[15] Kumar, R., Zhao, W., Singh, V. (2018). Joint time-frequency analysis of seismic signals: A critical review. Structural Durability & Health Monitoring, 12(2): 65. https://doi.org/10.3970/sdhm.2018.02329

[16] Santoso, S., Grady, W.M., Powers, E.J., Lamoree, J., Bhatt, S.C. (2000). Characterization of distribution power quality events with Fourier and wavelet transforms. IEEE Transactions on Power Delivery, 15(1): 247-254. https://doi.org/10.1109/61.847259

[17] Funabashi, T., Santoso, S., Grady, W.M., Powers, E.J., Lamoree, J., Bhatt, S.C. (2000). Discussion of "Characterization of distribution power quality events with Fourier and wavelet transforms" [Closure to discussion]. IEEE Transactions on Power Delivery, 15(4): 1343-1344. https://doi.org/10.1109/61.891565

[18] Yilmaz, A.S., Subasi, A., Bayrak, M., Karsli, V.M., Ercelebi, E. (2007). Application of lifting based wavelet transforms to characterize power quality events. Energy Conversion and Management, 48(1): 112-123. https://doi.org/10.1016/j.enconman.2006.05.003

[19] Subasi, A., Yilmaz, A.S., Tufan, K. (2011). Detection of generated and measured transient power quality events using Teager Energy Operator. Energy Conversion and Management, 52(4): 1959-1967. https://doi.org/10.1016/j.enconman.2010.11.006

[20] Cho, S.H., Jang, G., Kwon, S.H. (2009). Time-frequency analysis of power-quality disturbances via the Gabor-Wigner transform. IEEE Transactions on Power Delivery, 25(1): 494-499. https://doi.org/10.1109/TPWRD.2009.2034832

[21] Sahu, G., Dash, S., Biswal, B. (2020). Time-frequency analysis of power quality disturbances using synchroextracting transform. International Transactions on Electrical Energy Systems, 30(4): e12278. https://doi.org/10.1002/2050-7038.12278

[22] Grossmann, A., Morlet, J. (1984). Decomposition of Hardy functions into square integrable wavelets of constant shape. SIAM Journal on Mathematical Analysis, 15(4): 723-736. https://doi.org/10.1137/0515056

[23] Li, M., Wang, T., Kong, Y., Chu, F. (2021). Synchro-reassigning transform for instantaneous frequency estimation and signal reconstruction. IEEE Transactions on Industrial Electronics, 69(7): 7263-7274. https://doi.org/10.1109/TIE.2021.3100927

[24] Yu, G., Yu, M., Xu, C. (2017). Synchroextracting transform. IEEE Transactions on Industrial Electronics, 64(10): 8042-8054. https://doi.org/10.1109/TIE.2017.2696503

[25] Kumar, R., Sumathi, P., Kumar, A. (2017). Synchrosqueezing transform-based frequency shifting detection for earthquake-damaged structures. IEEE Geoscience and Remote Sensing Letters, 14(8): 1393-1397. https://doi.org/10.1109/LGRS.2017.2714428

[26] Daubechies, I., Lu, J., Wu, H.T. (2011). Synchrosqueezed wavelet transforms: An empirical mode decomposition-like tool. Applied and Computational Harmonic Analysis, 30(2): 243-261. https://doi.org/10.1016/j.acha.2010.08.002

[27] Rényi, A. (1961). On measures of entropy and information. In Proceedings of the Fourth Berkeley Symposium on Mathematical Statistics and Probability, pp. 547-562.

[28] Kumar, R., Singh, V., Ismail, M. (2023). Post-earthquake damage identification of buildings with LMSST. Buildings, 13(7): 1614. https://doi.org/10.3390/buildings13071614

[29] Auger, F., Flandrin, P. (1995). Improving the readability of time-frequency and time-scale representations by the reassignment method. IEEE Transactions on Signal Processing, 43(5): 1068-1089. https://doi.org/10.1109/78.382394